

**Joshua D. Davis<sup>1</sup>**

Robot and Protein Kinematics Laboratory,  
Department of Mechanical Engineering,  
Johns Hopkins University,  
Baltimore, MD 21218  
e-mail: jdavi160@jhu.edu

**Yunuscan Sevimli**

Robot and Protein Kinematics Laboratory,  
Department of Mechanical Engineering,  
Johns Hopkins University,  
Baltimore, MD 21218  
e-mail: yunus@jhu.edu

**Baxter R. Eldridge**

Robot and Protein Kinematics Laboratory,  
Department of Mechanical Engineering,  
Johns Hopkins University,  
Baltimore, MD 21218  
e-mail: beldrid1@jhu.edu

**Gregory S. Chirikjian**

Robot and Protein Kinematics Laboratory,  
Department of Mechanical Engineering,  
Johns Hopkins University,  
Baltimore, MD 21218  
e-mail: gregc@jhu.edu

# Module Design and Functionally Non-Isomorphic Configurations of the Hex-DMR II System

*Modular robots have captured the interest of the robotics community over the past several years. In particular, many modular robotic systems are reconfigurable, robust against faults, and low-cost due to mass production of a small number of different homogeneous modules. Faults in these systems are normally tolerated through redundancy or corrected by discarding damaged modules, which reduces the operational capabilities of the robot. To overcome these difficulties, we previously developed and discussed the general design constraints of a heterogeneous modular robotic system (Hex-DMR II) capable of autonomous team repair and diagnosis. In this paper, we discuss the design of each module, in detail, and present a new, novel elevator module. Then, we introduce a forest-like structure that enumerates every non-isomorphic, functional agent configuration of our system. Finally, we present a case study contrasting the kinematics and power consumption of two particular configurations during a mapping task.*

[DOI: 10.1115/1.4032273]

## 1 Introduction

Many researchers have designed modular, reconfigurable robots to adapt to environmental disturbances [1,2] and to increase reliability and robustness through repair processes [3]. Additionally, the cost of fielding multiple modules to form a robot can be offset by their simplistic nature and increased efficiency/life [4]. In general, modular robots can be split into two distinct groups (i.e., homogeneous or heterogeneous) depending on their specific morphologies. Homogeneous modular robotic systems comprise identical modules normally arranged in lattice or chain-like structures. These systems have been used to demonstrate reconfiguration between locomotion modes [5,6], self-assembly into complex structures, such as trusses or a six degree-of-freedom robot arm [7–11], and even transformations between one- and three-dimensional objects [12]. On the other hand, heterogeneous modular robots often employ homogeneous docking mechanisms and split capabilities across multiple modules [2,13]. In some of these systems, each module is itself an operational robot and the mating of several modules endows the system with additional capabilities or modes of locomotion [14,15].

In many cases, individual modular robots or agents are combined into cooperative multi-agent systems (CMSs) to complete more complex tasks. Of particular interest to researchers are exploration and mapping tasks in unstructured environments, such as unexplored, possibly hostile, buildings [16] and the surface of other planets [17]. Although additional team members (and hence modules) increase the probability of overall mission success, they also introduce more opportunities for system faults. According to Parker, some of the more common internal faults are individual robot (hardware) malfunctions, software errors or incompleteness, and communications failure [18]. Furthermore, Bjerknes and

Winfield claim that if these modular robots act as a swarm, overall reliability falls with an increasing number of agents in the absence of corrective behavior [19]. Most homogeneous modular robotic systems are designed to deal with these errors by identifying and discarding faulty modules [20] at the eventual cost of overall functionality.

In heterogeneous systems, fault recovery is more complex. Only recently have novel systems been developed that can replace individual modules to alter agent capabilities or replace damaged modules to effectively repair an agent. Bereton and Khosla introduced the first such system and it consisted of an agent with a forkliftlike manipulator and three replaceable subsystems [21]. Then, Kutzer et al. developed an entirely repairable modular system consisting of four heterogeneous modules connected together by rare-earth magnets. However, their work mainly concentrated on the diagnosis of faulty modules rather than the design of repairable ones [22]. Conversely, Ackerman and Chirikjian proposed necessary and sufficient design constraints for the development of a CMS capable of team repair and demonstrated a remotely assisted repair [23]. In Ref. [24], we furthered this work and presented the second-generation Hex-DMR system (Hex-DMR II) capable of autonomous team repair. (Video of the autonomous insertion and extraction repair processes are under the “[Supplemental Data](#)” tab in the ASME digital collection.) A general comparison between both systems is provided in Fig. 1.

Specifically, agents in the second-generation system are comprised of up to 12 replaceable modules arranged in radially symmetric layers. This layout enables the Hex-DMR II system to store additional modules that can either be used to augment capabilities (e.g., provide further tractive force, extend power capacity, and provide extra sensing) or have spare modules available for use in the repair process. At a minimum, each agent requires three drive modules, spaced evenly apart on the base layer, a power module, and a control module to achieve minimal functionality (i.e., blind locomotion). If an agent is also equipped with a sensing (camera) module and a manipulator module, it is further endowed

<sup>1</sup>Corresponding author.

Manuscript received September 14, 2015; final manuscript received December 9, 2015; published online May 4, 2016. Assoc. Editor: Venkat Krovi.

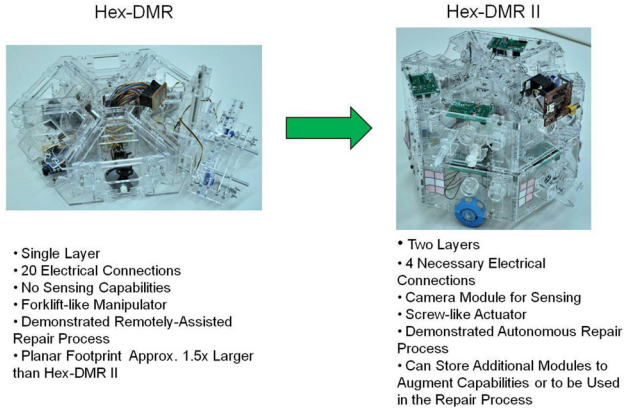


**Fig. 1 Comparison of the Hex-DMR systems**

with the ability to reconfigure or repair another agent (Fig. 2). An example of this process between a three-wheeled and a six-wheeled agent is graphically depicted in Fig. 3. Additionally, a sequence of stills from a trial experiment of the insertion process is included in Fig. 4. Modules can also be moved between layers with the aid of an elevator installed on a separate agent.

Since we previously demonstrated a robust repair process and discussed general design considerations for the Hex-DMR II system in Ref. [24], this paper instead elaborates on the design features and placement constraints of specific modules in the system.

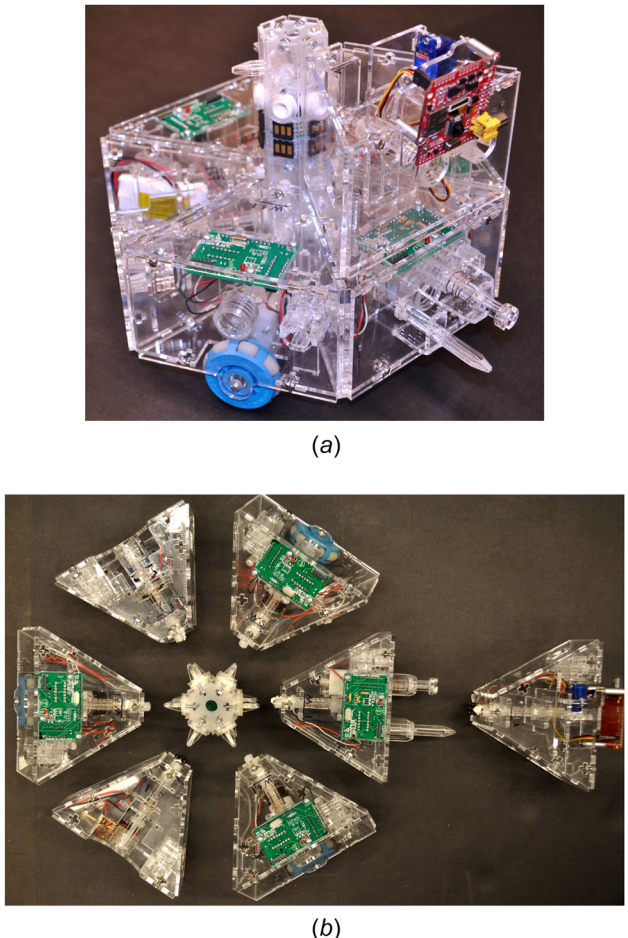


**Fig. 2 Views of an agent of the Hex-DMR II system: (a) isometric view of a repair agent of Hex-DMR II and (b) exploded view of a repair agent of Hex-DMR II**

We then identify four base configurations and generate configurational trees, based on non-isomorphic, functional agents, that fully describe all possible configurations of the system. Finally, we present an informative case study that compares the kinematic performance and power consumption of two base configurations.

## 2 Modules

The Hex-DMR II system was primarily designed to demonstrate an autonomous diagnosis and repair process through the use of heterogeneous modules. Although these module types were diversified to achieve specific capabilities, overarching hardware and mechanical structures were maintained to reduce overall cost and increase homogeneity. Moreover, core functions, such as manipulation, processing, and locomotion, were split across several different module types to limit the mechanical and electrical complexity of any given failure. Sections 2.1 and 2.2 highlight common features across modules and discuss specialized elements in each module type.

**2.1 Common Modular Features.** Two features extend to every module in the Hex-DMR II system. The first is the trapezoidal footprint that defines the perimeter of each module and the second is the docking mechanism which is essential for reconfiguring agents. In addition to these mechanical elements, every actuated module is equipped with a low-level control board for bidirectional motor control.

**2.1.1 Trapezoidal Footprint.** Each module (when excluding the central hub) has the same planar trapezoidal footprint. The individual height of each module may vary depending on installed components or function, but this distinction only affects possible agent configurations as opposed to overall geometry. This footprint is mainly a consequence of the hexagonal geometry of individual agents, which was thoroughly discussed in Ref. [24], but was also chosen due to three additional benefits.

First, during docking with the central hub, the two outer faces of adjacent modules help guide the manipulated module toward the preferred docking position. Second, the outer faces of docked modules are designed to be flush and coincident with one another which prevents the introduction of electrical noise through small, extraneous movements of the electrical connectors on the rear of modules during agent motion. Finally, the outer shell of each module, which forms the trapezoidal shape, is designed to be easily removable to enable quick access and replacement of internal components with minimal work. The shell and a majority of other mechanical components in the modules are constructed from laser-cut acrylic to increase modularity and ease of repair. To highlight the ease of assembly, a computer-aided design (CAD) representation of a fully deconstructed module is presented in Fig. 5.

**2.1.2 Docking Mechanism.** Modules in the Hex-DMR II system contain a simple docking mechanism based on a screw which enables a docking procedure utilizing only a single, actuated degree-of-freedom and also scales well to both smaller and larger applications. The central hub contains threaded inserts while every other module contains a central acrylic shaft with a conformally threaded “screw” which extends the length of each module. The screw and fasteners are coarsely threaded (3.15 threads/cm or 8 threads/in.) to reduce actuation times and to conserve energy. Furthermore, the screw and the corresponding insert were previously developed in Ref. [25] and were shown to reduce parts entropy while increasing fault tolerance to slight misalignments. On the opposite end of the shaft containing the screw, a rectangular extrusion is present that mates with the end-effector of the manipulator during actuation. A spring fashioned from 25 AWG copper wire extends between a collar on the shaft and a vertical support structure to ensure that contact is maintained with the end-effector during actuation. The shaft is supported by two

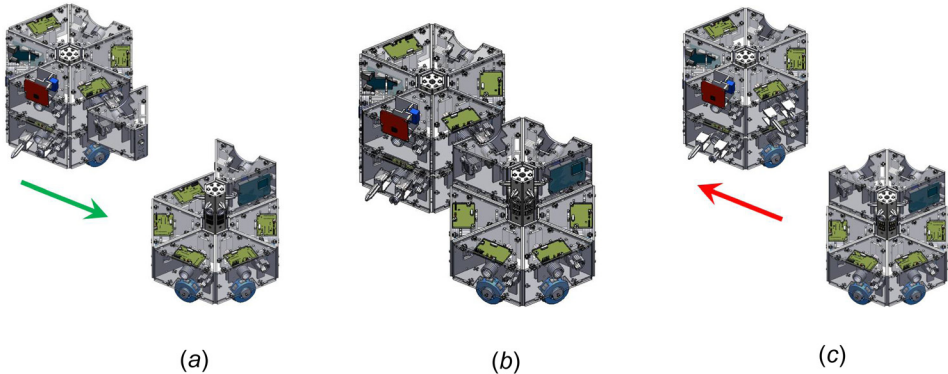


**Fig. 3** Graphical representation of the module insertion process: (a) driving forward to dock a module, (b) attaching a module to the central hub, and (c) driving backward to continue previous task

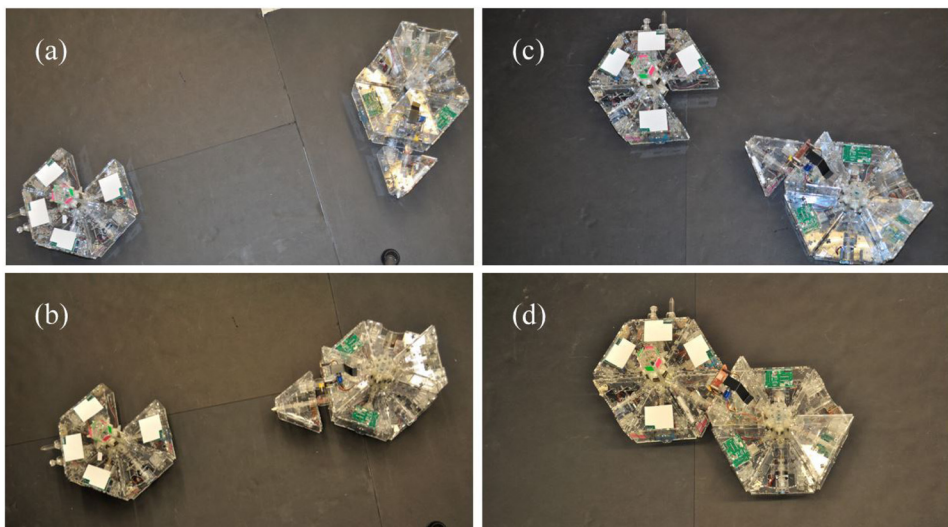


**Fig. 4** Stills from an experimental trial of the module insertion process: (a) the repair agent begins rotating clockwise until it senses the disabled agent, (b) the repair agent approaches the disabled agent and checks for a lack of module, (c) upon sensing a module, the repair agent rotates about the disabled agent until it faces a new module, and (d) the repair agent senses a lack of module and travels forward to insert the new module into the disabled agent, completing the repair process

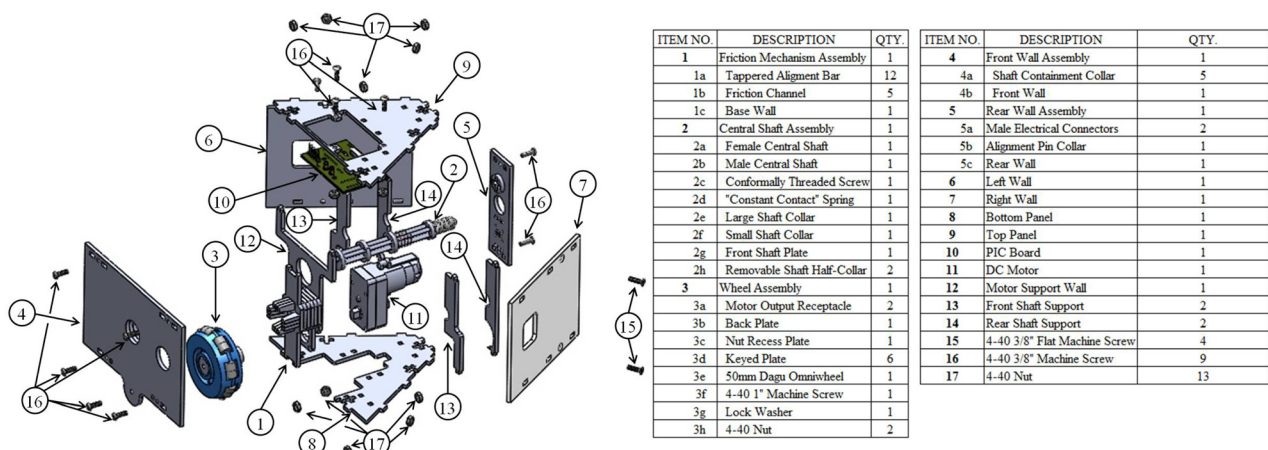


**Fig. 5** Exploded view of a module with its corresponding parts list

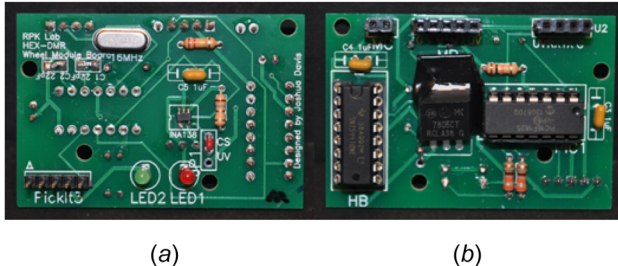


**Fig. 6 The PIC board: (a) top of board and (b) bottom of board**

vertical pieces of acrylic that extend throughout the interior of the module.

**2.1.3 Peripheral Interface Controller (PIC) Board.** Every actuated module in the Hex-DMR II system is installed with a custom-designed printed circuit board (PCB) called a “PIC board.” The main purpose of the PIC board, pictured in Fig. 6, is to interface with the control module and provide low-level motor control. Each PIC board is equipped with a PIC16F1825 microcontroller, a quadruple half-H driver (H-bridge) for bidirectional motor control, and two indicator light-emitting diodes (LEDs). The board is supplied 7.4 V through the electrical bus, and the PIC is supplied 5 V through a voltage regulator. The internal clock on the PIC tends to be fairly inaccurate and is subject to electrical noise; therefore, a clock signal from an external 16 MHz crystal oscillator was also provided.

The H-bridge is supplied regulated 5 V for logic comparisons and either regulated 5 V (for the manipulator module) or unregulated 7.4 V (for the other actuated modules) for driving the motor. Depending on the application, the H-bridge inputs are sent either a steady-state or pulse-width modulated (PWM) signal from the PIC. A single-stage low-pass filter (i.e., ceramic capacitor) was soldered across the motor leads (the H-bridge outputs) to reduce the electrical noise in the PIC’s serial communication lines.

The PIC board is installed on the top of each module so that the indicator LEDs are easily visible and that the leads for the in-circuit serial programmer are also accessible. The first indicator LED is green and has two specific functions. First, the LED indicates if the PIC board has power. Second, the LED blinks if the PIC board receives an invalid serial command which is helpful when diagnosing connection or baud rate issues. The second LED is red and blinks every time a byte is received by the PIC over serial communication.

**2.2 Modules Types.** In the current iteration of the Hex-DMR system, there are seven different types of modules that can be assembled to form an agent. Of these seven types of modules, four are required to field a minimally functional agent. The remaining three types of modules provide additional capabilities, such as sensing and manipulation to further augment the system. The general characteristics of these modules are summarized in Table 1,

**Table 1 Module types and physical characteristics**

Module type	Maximum dimensions			
	L (mm)	W (mm)	H (mm)	Mass (g)
Central hub	75.90	65.74	171.5	163
Elevator	116.1	132.0	185.9	537
Manipulator	179.0	132.0	82.55	257
Drive	116.1	132.0	117.8	262
Camera	125.3	132.0	116.4	234
Control	116.6	132.0	82.55	215
Power	116.1	132.0	82.55	225

while the specific design considerations for each module are discussed in Secs. 2.1.1–2.2.7.

**2.2.1 Central Hub.** The shape of the central hub is a byproduct of the choice of docking mechanism and the number of modules chosen to maximize the available surface area during docking given a minimum number of required modules on the base layer. As a result, the central hub took the form of a two-layer, hexagonal column (Figs. 7(a) and 8(a)). The main function of the central hub is to provide mechanical and electrical connections to the modules. Mechanical connections are achieved by screwing the shaft of the docking mechanism into a corresponding threaded insert located on the face of the central hub. A dual-purpose alignment pin is also present on each face of the central hub. During docking, the alignment pin helps correct small positional errors between the screw on the end of the docking mechanism and the insert on the central hub. Upon securing the module to the hub, the alignment pin constrains one of the module’s degrees-of-freedom and effectively prevents arbitrary rotations about the screw.

As modules are docked with the central hub, electrical connections are simultaneously established. Each docking location on the central hub is outfitted with two, three-pin female connectors. As the module is screwed into the hub, the spring-loaded male connectors, positioned on the rear face of the module, are pressed into the corresponding female connector establishing an electrical connection. Each pin on the male connector has 1.5 mm of travel resulting in semicompliant connections that increase robustness. The female connectors on the hub are augmented with brass c-channels to further increase robustness. Connections between modules are enabled by a custom-designed PCB (Fig. 9), which lies in the interior of the hub and is soldered to each female connector. Each layer on the central hub requires its own PCB and the PCBs are connected by ribbon cable.

Although the Hex-DMR II system is equipped with six separate electrical connections, only four are currently in use. Two connections are reserved for power, or the positive and negative terminals of the power module, two connections are used as transmission (TX) and reception (RX) lines for asynchronous serial communication, and the final two spare connections are for future development. These four main lines form the electrical bus for the Hex-DMR II system, and typical connections to the bus for a seven-module agent are depicted in Fig. 10.

**2.2.2 Elevator Module (E).** In Ref. [24], we highlighted the advantages of a multilayer system and briefly mentioned several theoretical options to transfer modules between levels. After careful consideration, we decided that an elevator module best preserved the homogeneity of the Hex-DMR II system as well as the completeness of repair. The resulting module is displayed in Figs. 7(b) and 8(b).

Unlike the other modules, the elevator module contains two docking mechanisms and occupies both layers on the central hub. Modules are manipulated between layers by first docking a module into a carriage on the left side of the elevator that contains a threaded insert. The carriage is placed in a vertical slotted track and holds a nut that travels along a threaded Acme rod when the geared direct current (DC) motor is actuated. For homogeneity and to lower cost, the motor was chosen to be the same as those used in the drive and manipulator modules. Due to limited spacing in the module, the DC motor was connected to the Acme rod, located on the opposite side of the module, by a gear train that maintained the original torque and motor speed. The thread spacing on the rod was selected to strike a balance between the torque required to lift a module and the speed at which the module would be lifted.

Electronically, the elevator is wired to and controlled by a PIC board that is identical to those installed in the other actuated modules. In addition, the elevator module is equipped with two infrared reflectance sensors that are positioned at the distal ends of the

vertical slot for the carriage. The analog outputs of the sensors are connected in parallel such that if the carriage sufficiently approaches either sensor, the signal dramatically drops and triggers the PIC board to stop the carriage.

**2.2.3 Manipulator Module (M).** The manipulator module (Figs. 7(c) and 8(c)) is the only module capable of removing or adding modules to either the central hub or elevator. During a

module extraction procedure, the manipulator module is aligned with and driven toward the second agent. As the manipulator is driven forward, a 39 mm alignment pin engages a conformal friction mechanism on the interior of the other module. The front of the alignment pin is tapered to enable successful mating with misalignment errors of up to 2.54 mm and 0.33 rad. The alignment pin also positions the end-effector in-line with the central shaft on the other module.

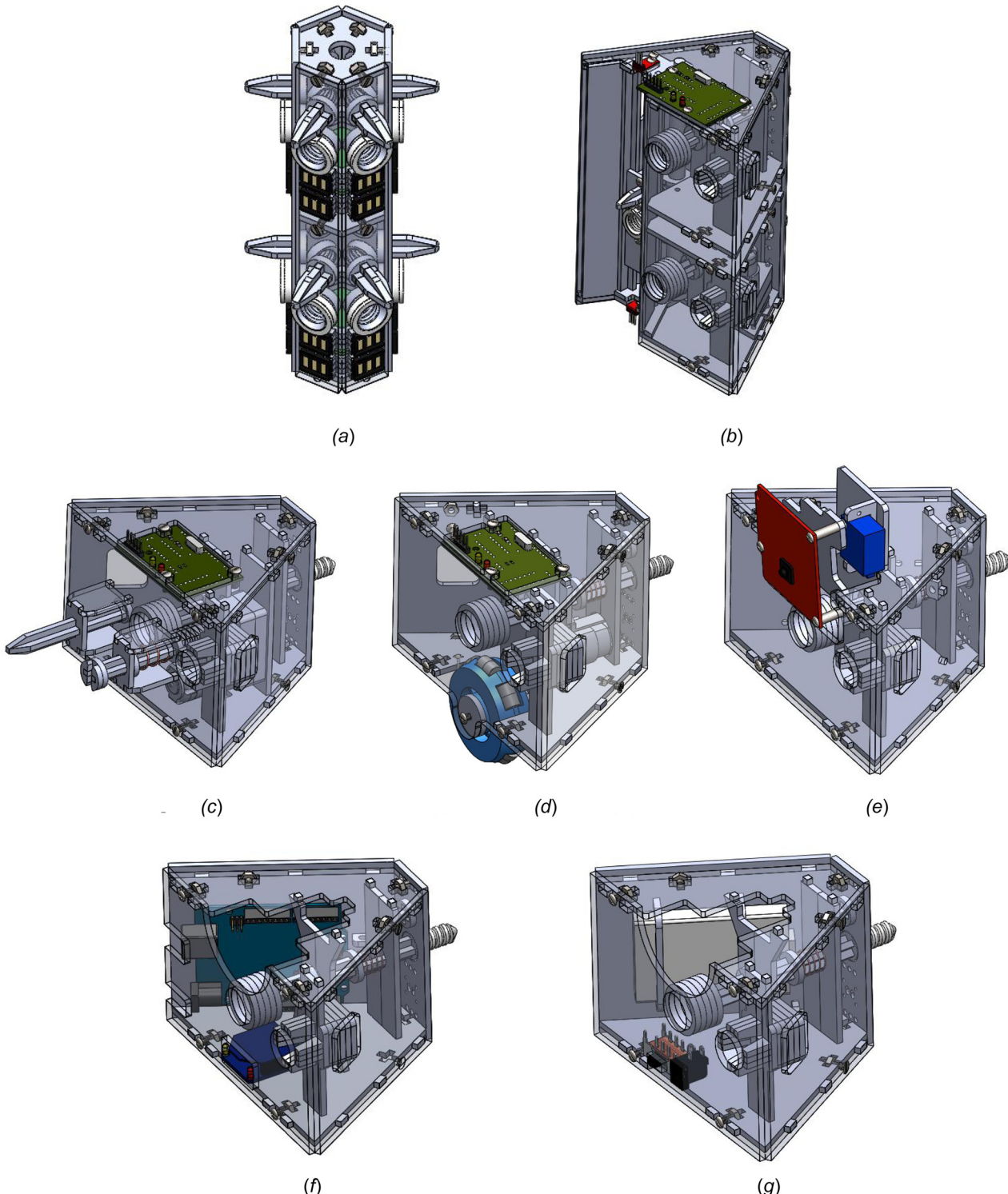


**Fig. 7 CAD representations of the types of modules for the Hex-DMR II system: (a) CAD central hub, (b) CAD elevator module (E), (c) CAD manipulator module (M), (d) CAD drive module (D), (e) CAD camera module ( $C_a$ ), (f) CAD control module (C), and (g) CAD power module (P)**

The front of the end-effector is outfitted with a recessed slot that is conformal to the rectangular extrusion on the central shaft when properly aligned. The end-effector also contains a 25 AWG copper wire along part of its length. This spring provides a normal force such that when the two shafts align they snap together. It also enables the end-effector to retreat into the manipulator as the shaft of the docking mechanism is unscrewed from the central

hub. Upon successful mating, the alignment pin provides sufficient friction to ensure that the other module is removed from the central hub when the manipulator drives away. The end-effector and alignment pin are positioned in such a manner that one manipulator module can remove another.

The manipulator is controlled by a PIC board that is equipped with an additional current sensor to terminate actuation. During

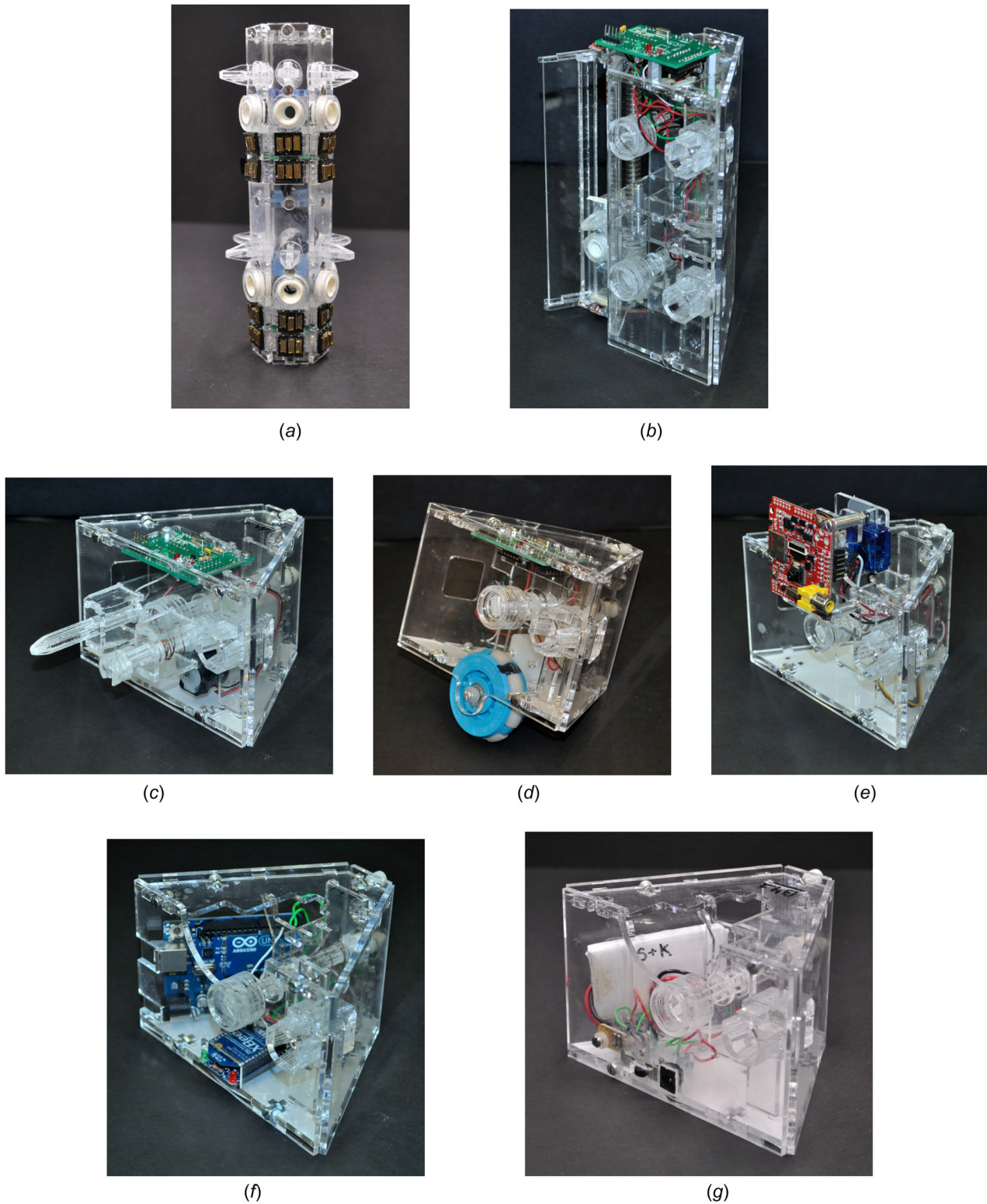


**Fig. 8** Hardware prototypes of modules for Hex-DMR II: (a) central hub, (b) elevator module (E), (c) manipulator module (M), (d) drive module (D), (e) camera module ( $C_a$ ), (f) control module (C), and (g) power module (P)

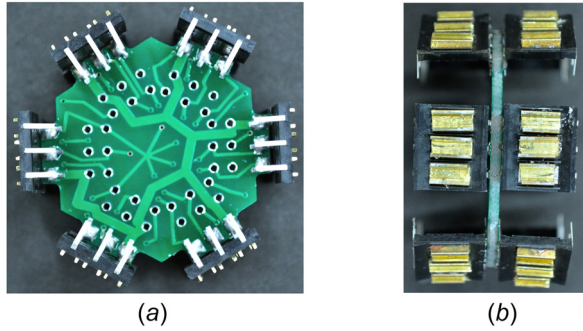


**Fig. 9 Central hub PCB with connections: (a) top view and (b) side view**

docking, the end-effector is stopped when the current reaches a steady plateau, above the nominal free rotation voltage, which indicates stalling or a completely docked module. During extraction, the PIC board instead waits for the current to drop to a steady-state, below a certain threshold, indicating free-rotation.

**2.2.4 Drive Module (D).** The drive module's (Figs. 7(d) and 8(d)) main purpose is to provide locomotion for agents in the Hex-DMR II system. Each drive module is equipped with a 49.2 mm diameter omnidirectional wheel. These wheels have eight cylindrical rubber rollers which allow sliding along the axial direction and still maintain the "no-slip" condition in the tangential direction. Although there are 7.5 mm gaps between each roller, each wheel maintains at least one point of contact with the ground at all times. The wheels are centered and located 12.9 mm from the front of the module. When drive modules are installed on the base layer of an agent, they provide an average of 30 mm of ground clearance. Moreover, when the drive modules are docked and spaced evenly apart, they distribute the center of mass toward the geometric center of the central hub yielding higher stability. The omnidirectional wheels are attached to a geared DC motor through a keyed acrylic shaft. The motors are driven through a PWM signal, specified by the control module, and generated by the microcontroller on the PIC board. The rotational speed of each motor is then adjusted by altering the duty cycle of the PWM signal.

**2.2.5 Camera Module ( $C_a$ ).** Currently, the camera module (Figs. 7(e) and 8(e)) provides the only sensing modality for the Hex-DMR II system. Since the main purpose of the Hex-DMR II system was to demonstrate a low-cost/low complexity, robust autonomous repair process, a CMUcam4 camera was selected. This camera provides simple color tracking and readily interfaces with the microcontroller in the control module, over serial communication, keeping control and initial development simple. The camera is mounted to a servomotor to increase the functional field of view by tilting. The camera is located on the top of the module and extends above and forward of the normal footprint. Therefore, the camera module can only be installed on the lower layer if a module is not present above it or on the upper layer.

**2.2.6 Control Module (C).** The control module (Figs. 7(f) and 8(f)) handles all decision-making for each agent in the Hex-DMR II system. The module is equipped with an ATmega168-20PU microcontroller for processing data and serial communication. The control module sends commands to the camera and actuated modules through the TX line on the electrical bus and receives information back on the RX line. In addition, the microcontroller is connected to an XBee wireless radio through a software serial protocol to communicate with other agents. The XBee radio is centered, below the central shaft, on the front of the module for easy access and removal. The top of the control module has a cutout to enable the storage of a drive module in the upper layer. Once the drive module is docked, the control module can only be removed after the drive module is removed.

**2.2.7 Power Module (P).** The power module (Figs. 7(g) and 8(g)) is effectively the second passive element in the Hex-DMR II system. At least one power module is required to field a functional agent; however, additional power modules may be added to achieve longer runtimes. Power modules have two separate modes of operation which are adjustable through a switch installed on the front of the module. The switch is partially recessed such that another agent cannot activate it. The first mode of operation supplies power to the agent, while the second mode isolates the battery and enables charging. The module also contains a DC power jack on the front of the module allowing easy access for charging. Each power module is equipped with one 800 mAh, 7.4 V Lithium-ion polymer battery. The battery is directly connected to the male electrical connections on the rear of the module. For extra precaution, and to prevent back-charging in the case of multiple batteries on an agent, a diode is placed in-line with the positive terminal. Similar to the control module, the power module has a cutout to enable storage of drive modules above it.

### 3 Agent Configurations

As mentioned previously, agents in the Hex-DMR II system are comprised up to 12 modules, arranged in two vertically stacked rings of six modules. Depending on the location, number, placement, and type of module, agents can be formed with vastly different capabilities. If there were no constraints on the placement of modules and we assumed that each module only occupied one layer there would be a possibility of  $6^{12}$  or  $2.18 \times 10^9$  configurations. Luckily, this is not the case.

In the remainder of this section, we discuss the underlying constraints for assembling functional agents from our set of modules. Then, we outline a method for enumerating possible agent configurations for certain base configurations and finally we present a case study comparing two base configurations for a specific task.

**3.1 Module Placement Constraints.** There are two types of constraints that guide the placement of modules. The first is a functional constraint and relates to the number of a certain type of module required for a minimally functional agent. The second is an interference constraint and relates to the geometry of surrounding modules which encroach into separate locations. The functional constraints for the Hex-DMR II system are as follows:

- (1) control module
- (1) power module
- (3) drive modules placed evenly apart on the base layer in a radially symmetric fashion

and the interference constraints are:

- Drive modules on the upper layer may only be placed above control or power modules.
- Camera modules may be placed on the lower layer only if another module is not present above it.
- Elevator modules must occupy both layers.

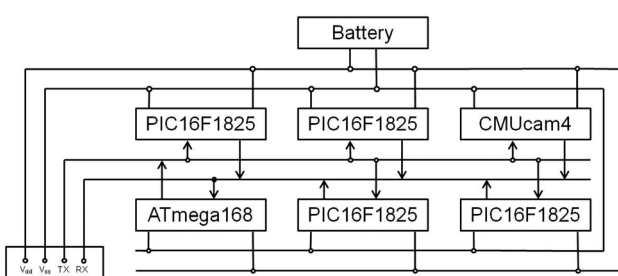


**Fig. 10 Electrical bus for a seven-module agent**

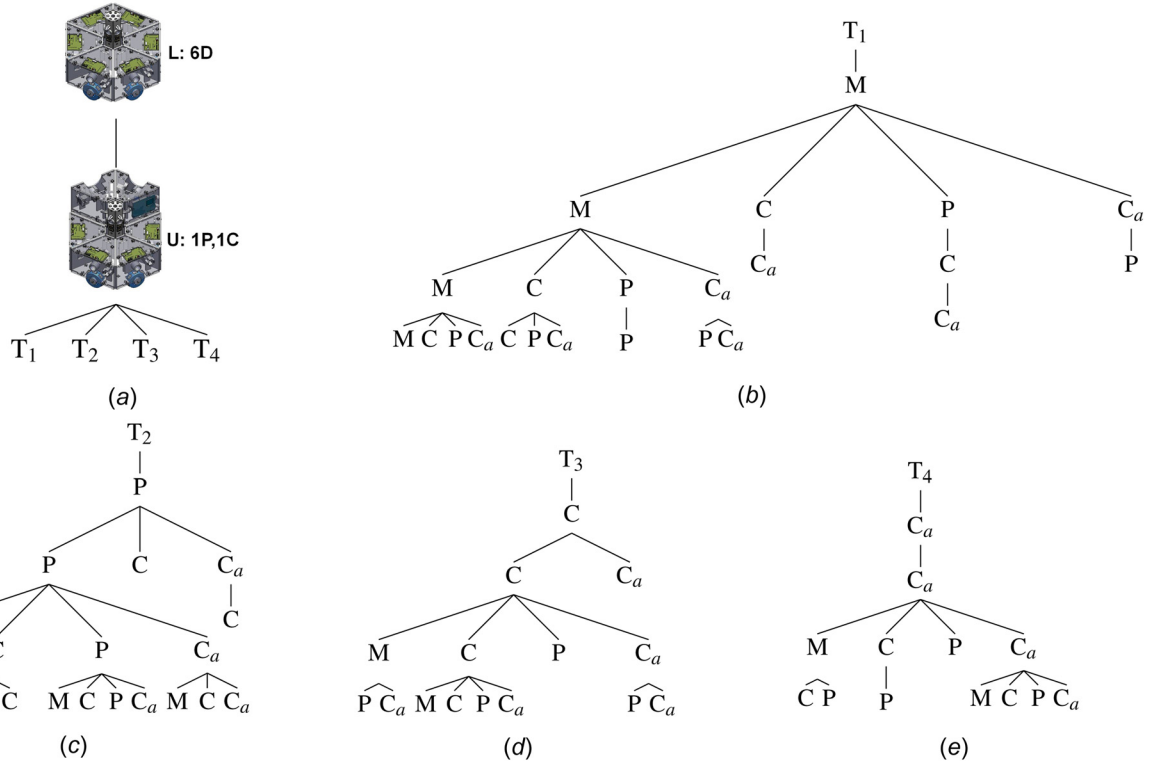


**Fig. 11 Configurational tree for the six-wheeled base configuration:** (a) main tree, (b) manipulator module subtree, (c) power module subtree, (d) control module subtree, and (e) camera module subtree

**3.2 Base Configurations.** Identifying all possible agent configurations can be a tedious and convoluted task. Separate studies, such as Ref. [26], provided a mathematical construct to enumerate all unique, non-isomorphic configurations of modular robotic systems. However, due to constraints on the placement of modules and the heterogeneity of our system we had to follow a slightly different approach. Therefore, we have broken down the task of identifying all non-isomorphic functional configurations into more manageable base configurations. A base configuration is defined as a set of drive modules positioned on the bottom layer of the agent. In a sense, drive modules can be thought of as a limiting case; at least three modules are necessary to achieve a holonomic drive and a maximum of six modules greatly constrains the remaining configurations.

For each base configuration, we construct a tree that details the type and location of subsequently added modules. We begin by adding either control and/or power modules to the root of the tree (the base configuration). This branch represents the first minimally functional agent and we can begin to enumerate subsequent configurations. Due to the radially symmetric nature of the Hex-DMR II system, we exclude module permutations on single layers from the count of unique agent configurations. The collection of trees for each base configuration forms a forest and clearly establishes all possible agent configurations. For our particular system, the six drive module base configuration yields the smallest number of overall agent configurations and the corresponding configuration tree is presented in Fig. 11, where  $T_i$  represents a placeholder between the main tree and subtrees and  $M, P, C$ , and  $C_a$  represent modules types. The first functional configuration is located at the first branch in Fig. 12 and each subsequent branch provides a new, unique configuration. In total, the Hex-DMR II system has 10,503 possible unique configurations. The specific breakdown per base configuration is provided in Table 2.

**3.3 Case Study.** With 10,503 possible agent configurations, choosing the proper configuration for a specific mission can be difficult. To give some insight into this process, we present a case study comparing a three-wheeled agent to a six-wheeled agent for a long-duration mapping task using a camera module. In this

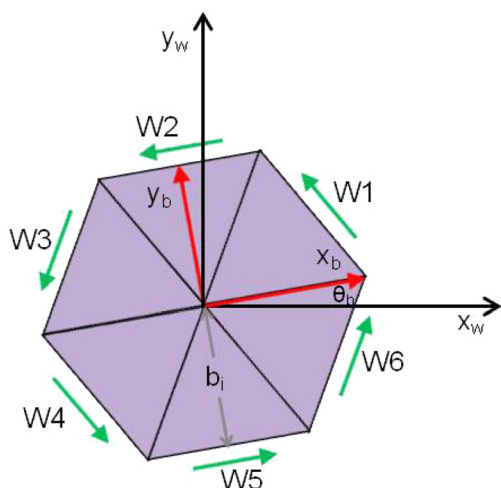


**Fig. 12 Coordinate reference frame for the kinematics**

**Table 2 Number of agent configurations per base configuration**

Base configuration	Number of configurations
3	7374
4	2467
5	592
6	70

particular case, it is assumed that only one agent is necessary and the primary failure mode is loss of power. Therefore, each agent is comprised of one control module, one camera module, and the proper number of drive modules. The remaining locations are filled with power modules. In this case study, we will theoretically examine the kinematic performance and power consumption of each agent as they execute a given trajectory.

**3.3.1 Configuration-Based Kinematics.** One of the key design elements of the Hex-DMR II system is that each agent can achieve holonomic motion in each of the base configurations. In fact, Indiveri presented a generalized method in Ref. [27] to derive the kinematics of a  $N$ -wheeled robot with omnidirectional wheels arranged in an arbitrary configuration assuming perfect rolling. Following this procedure, we derive the kinematic equations of motion for the three-wheeled configuration (W1, W3, and W5) according to the module orientations pictured in Fig. 13

$$\begin{bmatrix} \dot{x}_w \\ \dot{y}_w \\ \theta_w \end{bmatrix} = \begin{bmatrix} \cos(\theta_w) & -\sin(\theta_w) & 0 \\ \sin(\theta_w) & \cos(\theta_w) & 0 \\ 0 & 0 & 1 \end{bmatrix} \begin{bmatrix} \dot{x}_b \\ \dot{y}_b \\ \dot{\theta}_b \end{bmatrix} \quad (1a)$$

$$\begin{bmatrix} r_1 \dot{W}_1 \\ r_3 \dot{W}_3 \\ r_5 \dot{W}_5 \end{bmatrix} = \begin{bmatrix} -\frac{1}{2} & \frac{\sqrt{3}}{2} & b_1 \\ -\frac{1}{2} & -\frac{\sqrt{3}}{2} & b_3 \\ \frac{1}{2} & 0 & b_5 \end{bmatrix} \begin{bmatrix} \dot{x}_b \\ \dot{y}_b \\ \dot{\theta}_b \end{bmatrix} = T_3 \begin{bmatrix} \dot{x}_b \\ \dot{y}_b \\ \dot{\theta}_b \end{bmatrix} \quad (1b)$$

where Eq. (1a) transforms body velocities into world-frame velocities via a rotation matrix with an axis of rotation out-of-the-plane, and  $r_i$ ,  $b_i$ , and  $\dot{W}_i$  from Eq. (1b) are, respectively, the radius, distance from the wheel to the center of rotation, and velocity of the  $i$ th wheel. The kinematic equations of motions for the six-wheeled agent are

$$\begin{bmatrix} r_1 \dot{W}_1 \\ r_2 \dot{W}_2 \\ r_3 \dot{W}_3 \\ r_4 \dot{W}_4 \\ r_5 \dot{W}_5 \\ r_6 \dot{W}_6 \end{bmatrix} = \begin{bmatrix} -\frac{1}{2} & \frac{\sqrt{3}}{2} & b_1 \\ -1 & 0 & b_2 \\ -\frac{1}{2} & -\frac{\sqrt{3}}{2} & b_3 \\ \frac{1}{2} & -\frac{\sqrt{3}}{2} & b_4 \\ 1 & 0 & b_5 \\ \frac{1}{2} & \frac{\sqrt{3}}{2} & b_6 \end{bmatrix} \begin{bmatrix} \dot{x}_b \\ \dot{y}_b \\ \dot{\theta}_b \end{bmatrix} = T_6 \begin{bmatrix} \dot{x}_b \\ \dot{y}_b \\ \dot{\theta}_b \end{bmatrix} \quad (2)$$

Immediately, we note that  $T_6$  is not square and  $\text{rank}(T_6) = 3$  indicating that there is more than one set of wheel velocities that result in the same planar motion. However, due to the no-slip constraint only one such set of wheel velocities is valid and produces the correct holonomic motion. In fact, the correct set of velocities is found by noting that each wheel should have a nonzero velocity unless the unit axis normal to the rollers is solely along the direction of motion. Interestingly, the kinematics for the four- and five-wheeled agents can also be determined from Eq. (2) by eliminating the appropriate number of rows in  $T_6$  that correspond to the locations of the missing drive modules.

We can gain some insight into the kinematic performance of each base configurations by using Eqs. (1) and (2) to produce the proper wheel velocities to track an arbitrary trajectory Fig. 13 on flat, ideal terrain. The associated wheel velocities or inputs for each wheel are presented in Fig. 14.

From the results, we see that the wheel velocities in the three-wheeled and six-wheeled case are identical. Moreover, this trajectory was generated using the same agent velocity which indicates

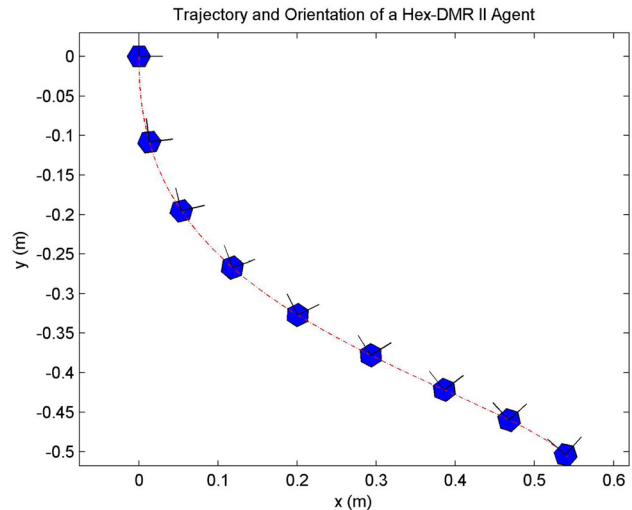


**Fig. 13 Trajectory for a Hex-DMR II agent**

that the number of drive modules does not contribute to agent speed. Therefore, the benefit of a six-wheeled configuration is mainly due to the tractive force provided by each additional wheel. Additionally, this tractive force should enable the six-

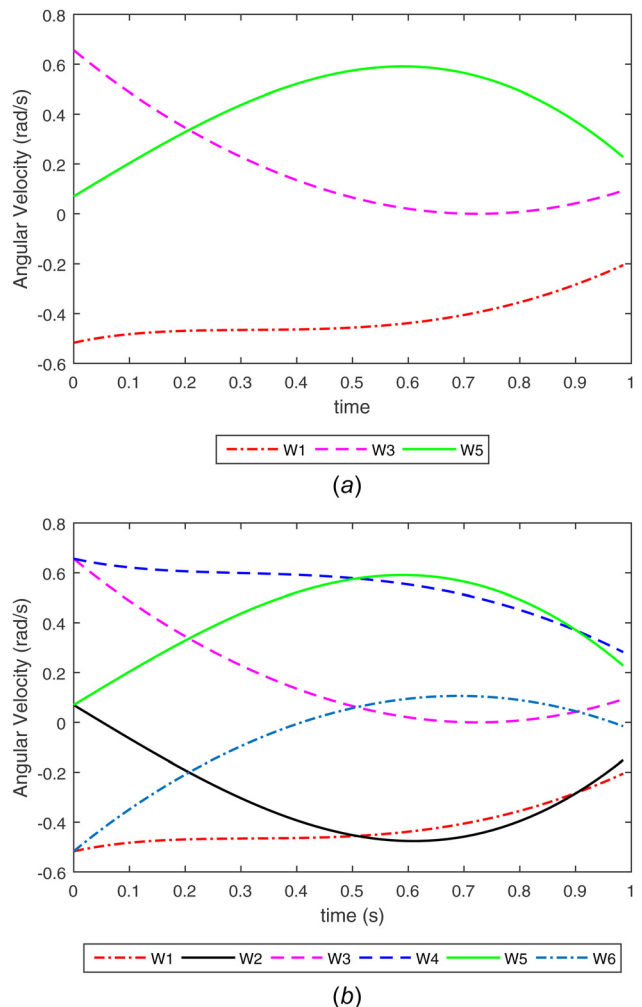


**Fig. 14 Wheel angular velocity inputs for the given trajectory: (a) angular velocities for a three-wheeled agent and (b) angular velocities for a six-wheeled agent**

wheeled configuration to climb slightly steeper terrain than its three-wheeled counterpart.

Another benefit of the six-wheeled agent is that additional drive modules increase the number of contact points with the ground simultaneously improving stability at the cost of increasing overall friction (mostly internally) and power consumption. If we were to assume more realistic conditions, the six-wheeled configuration offers one final advantage. Consider a situation when the agent loses traction (gets stuck) in a particular location. Although the three-wheeled and six-wheeled configurations can perform the same holonomic maneuvers, the six-wheeled configuration can realize approximately octuple the amount of random wheel motions (including paired wheel motions) to try to free itself, effectively improving its probability of mission success.

**3.4 Experimental Validation.** To test our claims related to the maximum tractive force and the angle of incline that each agent could climb, we conducted two separate experiments. The first measured the maximum tractive force of each agent by attaching a linear, spring-loaded force gauge to each central hub and then commanding each agent to drive forward (at the same speed) on a flat, level surface. This process was repeated five times, on three separate surfaces, and the average force generated by each agent as well as the ratio of forces between the two agents were recorded in Table 3. Additionally, a picture of the experimental setup was included in Fig. 15.

When we average these three ratio data points, we see that the six-wheeled agent has approximately 1.63 times more tractive force than the three-wheeled agent. We believe that two factors contributed to this value being smaller than the expected value of 2. First, during testing we observed that the six-wheeled configuration slipped on occasion, which limited the maximum tractive force of the agent. This slipping was most likely caused by poor contact between the ground and the wheels. Since the six-wheeled agent has six points of contact and only three points are necessary to define a plane, if one of the wheels was slightly misaligned it would be lifted off of the ground. Also, if we assumed that every wheel was in contact with the ground then each wheel is subject to a different normal force due to the nonsymmetric mass distribution of the robot. We believe the second cause can be attributed to internal friction in the drive modules which is mainly due to the connection between the drive shaft and the front acrylic panel of the module.

Our second experiment sought to quantify and validate our claim that a six-wheeled agent can climb steeper terrain than a three-wheeled agent. To do so, we commanded both agents to climb an inclined platform multiple times. A successful trial, at a specific incline, was marked by the agent being able to move forward after starting at a complete standstill. After each trial, the incline was increased and the experiment was repeated until the agent could no longer move forward. As expected, the results indicated that the six-wheeled agent could climb an incline 6 deg or 1.67 times steeper than the three-wheeled agent. Specifically, the six-wheeled agent climbed a slope of 14 deg 19' 12 in. and the three-wheeled agent climbed a slope of 8 deg 31' 48 in.

It is important to note that due to a lack of completed battery modules, the three-wheeled agent was configured slightly

differently than described in Sec. 3.3 (i.e., it contained three battery modules, two manipulator modules, and three control modules). In fact, the configured agent was 44 g more massive than the described agent and this additional weight would imply that the three-wheeled agent could climb a slightly steeper slope (possibly up to a half a degree more). We should also mention that although this test was only carried out on only one surface, the basic claim that the six-wheeled agent can climb steeper terrain than the three-wheeled agent should generalize to other solid surfaces with similar coefficients of friction.

**3.4.1 Power Consumption.** Although the six-wheeled configuration appears to achieve better kinematic performance, we must be mindful of the resulting power consumption. Power consumption, or more accurately current draw, of each module type was experimentally measured for an operational agent. The power module was assumed to provide no contribution, while the camera and control modules were assumed to have a constant draw. The current draw of the drive modules was measured at eight different angular velocities as well as in an idle state. A second-order polynomial was fit to the measurements to generate current draw across all possible angular velocities. Using these data points, the current draw over the trajectory was simulated for both of the base configurations.

As expected, the simulation revealed that the six-wheeled agent drew twice the amount of current. If we were to arbitrarily assume that this trajectory took 1 min to complete, the three-wheeled agent could complete approximately 375 iterations and the six-wheeled configuration could only complete approximately 121 iterations.

Thus, for this particular mission there is a very obvious trade-off between the two configurations. The three-wheeled configuration is capable of operating approximately 3.1 times as long as the six-wheeled configuration. However, the six-wheeled configuration can traverse steeper terrain, achieve better stability, and possibly overcome partial loss of traction more easily. Ideally, each agent would be reconfigured to maximize efficiency and minimize power consumption over the course of the mission.

## 4 Conclusions and Future Work

As CMSs become more prevalent and are introduced into harsher environments, efforts to design adaptive capabilities and to improve reliability/robustness are critical. One step toward a solution is to develop modular reconfigurable systems that react to environmental demands. To this end, we presented the Hex-DMR II system which is capable of autonomous team repair. Specifically, we discussed the design features and capabilities of each module type in detail. These modules were then organized into four base configurations which were used to generate unique configurational trees. These trees can then be combined into an easily searchable forest that delineates all possible agent configurations

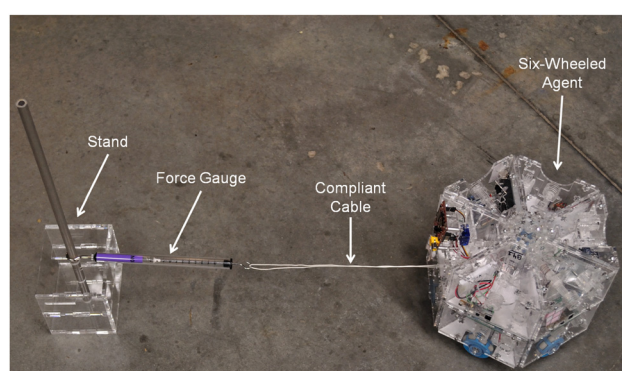


**Fig. 15 Experimental setup for measuring the maximum tractive force on concrete**

**Table 3 Maximum tractive force of a three-wheeled and six-wheeled agent**

Type of surface	Tractive force (N)		
	Three-wheel configuration	Six-wheel configuration	Ratio
Concrete	6.72	11.04	1.64
Tile	7.20	11.68	1.62
Wood	7.20	11.60	1.61

for the Hex-DMR II system. Finally, we presented a brief case study to gain insight into the advantages and disadvantages of particular base configurations for a general mission.

Ultimately, agent configurations should be chosen to satisfy mission requirements while simultaneously maximizing system lifetime utilizing the Hex-DMR II system's novel agent repair capabilities. To do so, we plan to develop algorithms, similar to Ref. [28], that search our configurational forest to determine configurations that fulfill certain parameters associated with particular missions. In addition, we will develop a second algorithm that determines the repairability of a given team of agents (i.e., how many random module failures can be tolerated before mission failure). By combining both algorithms, we can construct a team that is not only best-suited for a particular task but also the most robust against unexpected faults.

## Acknowledgment

The authors would like to thank M. Kendal Ackerman for his initial conceptualization of the Hex-DMR system and his insights while preparing this work. This work was supported by NSF Grant No. RI-Medium: 1162095. In addition, the work of Joshua Davis was supported by an ARCS Foundation Scholarship. Chirikjian's contribution to this material is based upon the work supported by (while serving at) the National Science Foundation as an IPA under the IR/D program. Any opinion, findings, and conclusions or recommendations expressed in this material are those of the authors and do not necessarily reflect the views of the National Science Foundation.

## References

- [1] Schwager, M., Dames, P., Rus, D. R., and Kumar, V., 2011, "A Multi-Robot Control Policy for Information Gathering in the Presence of Unknown Hazards," 15th International Symposium on Robotics Research (ISRR 11), Flagstaff, AZ, Aug. 28–Sept. 1.
- [2] Pagala, P., Ferre, M., and Armada, M., 2014, "Design of Modular Robot System for Maintenance Tasks in Hazardous Facilities and Environments," First Iberian Robotics Conference (ROBOT2013), Madrid, Nov. 28–29, pp. 185–197. pp. 185–197.
- [3] Bereton, C., and Kholas, P., 2002, "An Analysis of Cooperative Repair Capabilities in a Team of Robots," IEEE International Conference on Robotics and Automation (ICRA '02), Washington, DC, May 11–15, pp. 476–482.
- [4] Cao, Y., Fukunaga, A., and Kahng, A., 1997, "Cooperative Mobile Robotics: Antecedents and Directions," *Auton. Robot.*, **4**(1), pp. 7–27.
- [5] Davey, J., Kwok, N., and Yim, M., 2012, "Emulating Self-Reconfigurable Robots: Design of the SMORES System," IEEE/RSJ International Conference on Intelligent Robots and Systems (IROS), Vilamoura, Portugal, Oct. 7–12, pp. 4148–4153.
- [6] Zhao, J., Cui, X., Zhu, Y., and Tang, S., 2011, "A New Self-Reconfigurable Modular Robotic System UBot: Multi-Mode Locomotion and Self-Reconfiguration," IEEE International Conference on Robotics and Automation (ICRA), Shanghai, May 9–13, pp. 1020–1025.
- [7] Kutzer, M., Moses, M., Brown, C. Y., Scheidt, D. H., Chirikjian, G. S., and Armand, M., 2010, "Design of a New Independently-Mobile Reconfigurable Modular Robot," IEEE International Conference on Robotics and Automation (ICRA), Anchorage, AK, May 3–7, pp. 2758–2764.
- [8] Gilpin, K., Kotay, K., Rus, D., and Vasilescu, I., 2008, "Miche: Modular Shape Formation by Self-Disassembly," *Int. J. Rob. Res.*, **27**(3–4), pp. 345–372.
- [9] Hossain, S., Nelson, C., Chu, K., and Dasgupta, P., 2014, "Kinematics and Interfacing of ModRED: A Self-Healing Capable, 4DOF Modular Self-Reconfigurable Robot," *ASME J. Mech. Rob.*, **6**(4), p. 041017.
- [10] Wei, H., Chen, Y., Tan, J., and Wang, T., 2011, "Sambot: A Self-Assembly Modular Robot System," *IEEE/ASME Trans. Mechatronics*, **16**(4), pp. 745–757.
- [11] Spröwitz, A., Moekel, R., Vespignani, M., Bonardi, S., and Ijspeert, A. J., 2014, "Roombots: A Hardware Perspective on 3D Self-Reconfiguration and Locomotion With a Homogeneous Modular Robot," *Rob. Auton. Syst.*, **62**(7), pp. 1016–1033.
- [12] Yim, S., and Sitti, M., 2013, "SoftCubes: Towards a Soft Modular Matter," IEEE International Conference on Robotics and Automation (ICRA), Karlsruhe, Germany, May 6–10, pp. 530–536.
- [13] Lyder, A., Stoy, K., Garcia, R. F. M., Larsen, J. C., and Hermansen, P., 2013, "On Sub-Modularization and Morphological Heterogeneity in Modular Robotics," 12th International Conference on Intelligent Autonomous Systems (IAS), Jeju Island, South Korea, June 26–29, pp. 649–661.
- [14] Kernbach, S., Schlahter, F., Humza, R., Liedke, J., Popesku, S., Russo, S., Ranzani, T., Manfredi, L., Stefanini, C., Matthias, R., Schwarzer, Ch., Girault, B., Alschbach, P., Meister, E., and Scholz, O., 2011, "Heterogeneity for Increasing Performance and Reliability of Self-Reconfigurable Multi-Robot Organisms," IROS11 Workshop on Robotics for Neurology and Rehabilitation, San Francisco, CA, Sept. 30, available at <http://arxiv.org/abs/1109.2288>
- [15] Hartono, P., and Nakane, A., 2011, "Robotics Modules With Realtime Adaptive Technology," *Int. J. Comput. Inf. Syst. Ind. Manage. Appl.*, **3**, pp. 185–192.
- [16] Howard, A., Parker, L., and Sukhatme, G., 2013, "Experiments With a Large Heterogeneous Mobile Robot Team: Exploration, Mapping, Deployment and Detection," *Int. J. Rob. Res.*, **25**(5–6), pp. 431–447.
- [17] Roehr, T., Cordes, F., and Kirchner, F., 2013, "Reconfigurable Integrated Multi-robot Exploration System: Heterogeneous Modular Reconfigurable Robots for Space Exploration," *J. Field. Rob.*, **31**(1), pp. 3–34.
- [18] Parker, L., 2012, "Reliability and Fault Tolerance in Collective Robot Systems," *Handbook on Collective Robotics: Fundamentals and Challenges*, Pan Stanford Publishing, Singapore.
- [19] Bjørknes, J., and Winfield, A., 2013, "On Fault Tolerance and Scalability of Swarm Robotic Systems," *Distrib. Auton. Rob. Syst.*, **83**, pp. 431–444.
- [20] Fei, Y., and Wang, C., 2014, "Self-Repairing Algorithm of Lattice-Type Self-Reconfigurable Modular Robots," *J. Intell. Rob. Syst.*, **75**(2), pp. 193–203.
- [21] Bereton, C., and Kholas, P., 2000, "Towards a Team of Robots With Repair Capabilities: A Visual Docking System," 7th International Symposium on Experimental Robotics (ISER 2000), Waikiki, HI, Dec. 11–13, pp. 333–342.
- [22] Kutzer, M., Armand, M., Schied, D., Lin, E., and Chirikjian, G., 2008, "Toward Cooperative Team-Diagnosis in Multi-Robot Systems," *Int. J. Rob. Res.*, **27**(9), pp. 1069–1090.
- [23] Ackerman, M., and Chirikjian, G., 2012, "Hex-DMR: A Modular Robotic Test-Bed for Demonstrating Team Repair," IEEE International Conference on Robotics and Automation (ICRA), St. Paul, MN, May 14–18, pp. 4464–4469.
- [24] Davis, J., Sevimli, Y., Ackerman, M., and Chirikjian, G., 2016, "A Robot Capable of Autonomous Robotic Team Repair: The Hex-DMR II System," *Advances in Reconfigurable Mechanisms and Robots II*, Springer, Cham, Switzerland, pp. 619–631.
- [25] Moses, M., Ma, H., Wolfe, K., and Chirikjian, G., 2014, "An Architecture for Universal Construction Via Modular Robotic Components," *Rob. Auton. Syst.*, **62**(7), pp. 945–965.
- [26] Chen, I., and Burdick, J., 1998, "Enumerating the Non-Isomorphic Assembly Configurations of Modular Robotic Systems," *Int. J. Rob. Res.*, **17**(7), pp. 702–719.
- [27] Indiveri, G., 2009, "Swedish Wheeled Omnidirectional Mobile Robots: Kinematics Analysis and Control," *IEEE Trans. Rob.*, **25**(1), pp. 164–171.
- [28] Kernbach, S., 2013, "Heterogeneous Self-Assembling Based on Constraint Satisfaction Problem," *Distrib. Auton. Rob. Syst.*, **83**, pp. 491–503.